KFUPM
Journal of Undergraduate Research International

Diamond Open Access

Article
Electrical Engineering/Industrial Engineering

Adaptive Velocity PSO-Based Parameter Optimization for a Permanent Magnet DC Motor Drive in Light Electric Vehicles

Mohammed Aldhaif Allah[1] and Moustafa Magdi Ismail[2*]

Cite https://doi.org/10.64589/juri/209733

Submitted: May 12, 2025 **Revised:** August 04, 2025 **Accepted:** August 20, 2025

ABSTRACT

This study presents an adaptive velocity particle swarm optimization (AVPSO) approach for tuning the proportional–integral (PI) controllers of a permanent magnet DC (PMDC) motor drive in light electric vehicles (LEVs). The objective is to enhance dynamic response, tracking accuracy, and stability under varying operating conditions. The proposed algorithm improves on classical particle swarm optimization (PSO) by adaptively adjusting inertia weight and acceleration coefficients, thereby achieving a better balance between exploration and convergence. A MATLAB/Simulink model is developed for offline evaluation, where the optimization process minimizes steady-state and transient errors in motor speed and armature current. Simulation results demonstrate that AVPSO achieves faster settling times, with reductions of 15.6% in forward operation and 2.1% in reverse, while eliminating steady-state errors present in classical PSO. Comparative analysis under four-quadrant operation and torque disturbance scenarios confirms that the AVPSO-based tuning improves current tracking, reduces power losses, and ensures stable performance across dynamic transitions. The findings highlight the effectiveness of AVPSO in enhancing control quality without compromising efficiency, offering a robust and scalable solution for LEV motor drive applications.

Keywords: adaptive velocity PSO, permanent magnet DC motor, off-line tuning parameters, optimization control, motor drive, light electric vehicles

1. INTRODUCTION

Light electric vehicles (LEVs), including e-bikes, e-scooters, e-rickshaws, golf carts, and compact delivery vehicles, are increasingly adopted for urban mobility due to their environmental advantages, affordability, and suitability for short-distance, low-speed applications[1]. These vehicles require propulsion systems that are compact, efficient, and easy to control. Among various motor technologies, direct current (DC) motors particularly in brushed, brushless, and permanent magnet configurations remain a practical choice for LEVs due to their simple construction, smooth torque control, and minimal electronic complexity[2].

DC motors are widely used not only in propulsion systems, such as wheel hub motors[3], but also in auxiliary functions including electric power steering, ventilation, heating, and actuators for windows and seats[4]. For high-performance and larger electric vehicles (e.g., cars and buses), alternating current (AC) machines such as induction motors and permanent magnet synchronous motors (PMSMs) are preferred for their higher efficiency, speed capabilities, and regenerative braking support[5,6]. Nevertheless, for light-duty and cost-sensitive applications, DC motors continue to offer an optimal balance between functionality and system simplicity.

Recent advancements in motor drive control have emphasized optimization strategies for improving system performance under dynamic conditions[13–19]. For example, Xu et al. proposed an adaptive velocity particle swarm optimization (AVPSO) method to enhance flux-weakening control in permanent magnet synchronous motor drives[13]. The technique demonstrated reduced steady-state error and improved transient performance compared to gain parameters tuned using trial-and-error methods[13]. Other works have employed similar techniques to reduce torque ripple in surface-mounted PMSMs and optimize controller parameters using genetic algorithms[20]. Beyond motor control, AVPSO has also been successfully applied to maximum power point tracking in photovoltaic systems under no uniform irradiation conditions, as demonstrated by Zhang et al., yielding superior tracking speed and accuracy[21].

The main contribution of this study is the development of an off-line optimization strategy based on AVPSO for tuning the cascaded PI controllers of permanent magnet DC (PMDC) motor drives in light electric vehicles. Unlike conventional tuning methods that rely on manual adjustments and perform poorly under dynamic conditions, the proposed approach simultaneously optimizes four PI gains two for the inner current loop and two for the outer speed loop. The proposed AVPSO algorithm adaptively adjusts its search parameters to enhance convergence and solution quality. This results in notable improvements in dynamic response, tracking accuracy, and robustness over the traditional PSO algorithm presented in this work.

Table 1. *Comparison of DC motor types for electric vehicle applications*

Motor Type	Advantages	Disadvantages	Suitability for EV
Permanent Magnet DC [2]	- Compact size - High efficiency - High torque at low speed - Simple construction	- Limited power range - Poor heat dissipation - Expensive rare-earth magnets	Highly suitable for light EVs due to simplicity, easy control, and efficiency
Separately Excited DC Motor [3]	- Independent control of field and armature - Excellent speed and torque control - High dynamic response	- Requires two power sources - Complex - Higher cost and maintenance	Partially suitable for research or high-performance EVs, but less practical for consumer use
Shunt Self-Excited DC Motor [8]	- Stable speed regardless of load - simple speed regulation	- Lower starting torque - Not ideal for variable load	Not suitable, not ideal for frequent start-stop or acceleration requirements in EVs
Series Self-Excited DC Motor [9]	- Very high starting torque - Simple construction - simple for traction	- Poor speed regulation - Risk of overspeed in no load - Maintenance-intensive (brushes)	Historically used in older EVs or trams, but not preferred now due to control and safety limitations
Short Compound DC Motor [10]	- Balanced between torque and speed regulation - Better load handling than shunt	- More complex than shunt/series - Still not efficient for EVs	Limited suitability, complexity not justified for LEVs
Long Compound DC Motor [11]	- Improved torque and regulation - Better handling under dynamic loads	- Bulkier - More losses - Costlier	Rarely used in EVs today due to inefficiency and size
Cumulative Compound Motor [11]	- Combines advantages of series and shunt - Better performance under varying loads	- Moderate complexity - Larger footprint	Some suitability for heavier EVs, but still less efficient than PMDC or brushless types
Differential Compound Motor [11]	-Not suitable for EV applications	- Risk of instability under load - Torque drops with increased load (not desirable)	Not suitable for EV applications

The method is particularly effective in four-quadrant operation and torque disturbance scenarios, offering a computationally efficient and scalable solution for advanced LEV propulsion systems.

The remainder of this paper is organized as follows. Section 2 reviews related works relevant to motor drive optimization and PI controller tuning. Section 3 presents the modeling of the proposed LEV system, including the PMDC motor and the cascaded PI control strategy. Section 4 describes the methodology, focusing on the development of the Adaptive Velocity Particle Swarm Optimization (AVPSO) algorithm for optimal PI parameter tuning. Section 5 provides the results and discussion, including the simulation setup, performance evaluation, and comparative analysis between AVPSO, classical PSO, and existing PSO-based methods. Finally, Section 6 concludes the paper by summarizing the main findings and outlining potential directions for future research.

2. RELATED WORK

Tables 1 and 2 provide a comparative overview of DC motor types relevant to electric vehicle applications. Table 1 highlights technical attributes such as efficiency, torque capability, and maintenance requirements, while Table 2 outlines common real-world use cases and defining features like cost, reliability, and control complexity. Together, these tables support informed motor selection based on application-specific requirements in the EV industry.

3. METHODOLOGY

3.1. Modeling the proposed drive system of the PMDC motor. The objective of this study is to enhance the control system of LEVs to achieve better performance and reliability. Figure 1 presents the overall LEV architecture, which con-

Table 2. *Comparison of DC Motor types in EV applications*

Motor Type	Common Use	Key Features
Brushed DC (BDC)	Low-cost LEVs, toys, small EVs	Simple, low cost, high maintenance [11]
Brushless DC	E-bikes, scooters, hub motors	Efficient, reliable, requires electronic controller [12]
PMDC	Lightweight EVs, power assist systems	High torque, compact, simple [12]
Series DC Motor	Older EV designs	High starting torque, less efficient [8]

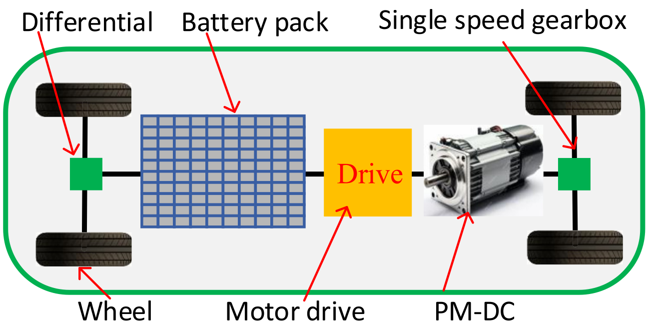

Figure 1. Main components of LEV system

sists of a motor drive, electric machine, battery pack, fixed-speed gearbox, and driving wheels. The traction motor, selected as a PMDC type powered by a Li-ion battery pack, is the primary focus of this work 19. The motor drive also incorporates the electrical circuit and charging system of the EV, where a DC/DC boost converter regulates power flow to ensure efficient energy conversion. This section therefore outlines the complete structure of the proposed LEV drive system.

The control system for the PMDC motor employs a cascaded PI control strategy consisting of two loops: an outer speed loop and an inner current loop, as shown in Figure 2. Meanwhile, the outer PI controller is responsible for tracking the reference angular velocity by generating a reference current signal. In contrast, the inner PI controller regulates the armature current by driving the voltage applied to the motor armature.

For beginning with, the electrical dynamics of the PMDC motor are derived from Kirchhoff Voltage law, expressed as:

$$v_a = R_a i_a + L_a \frac{d}{dt} i_a + K_e \omega \tag{1}$$

where v_a is the applied armature voltage, R_a and L_a are the armature resistance and inductance respectively, i_a is the armature current, and ω is the angular velocity of the motor. K_e is the back electromotive force constant.

In parallel, the inner PI controller generates a control voltage v_a based on the difference between the reference and actual armature currents:

$$v_a = K_{pi}(i_{a\text{-ref}} - i_a) + K_{ii} \int (i_{a\text{-ref}} - i_a)\, dt \tag{2}$$

where K_{pi} and K_{ii} are the proportional and integral gains of the current controller, and i_{a_ref} is the current reference signal provided by the speed loop.

In sequence, the outer PI controller generates the current reference i_{a_ref} by comparing the desired and actual angular velocities:

$$i_{a\text{-ref}} = K_{p\omega}(\omega_{ref} - \omega) + K_{i\omega} \int (\omega_{ref} - \omega)\, dt \tag{3}$$

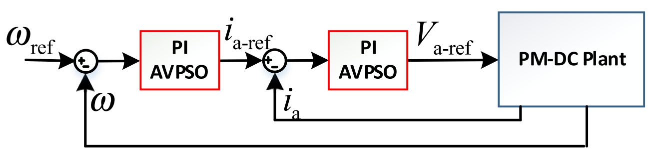

Figure 2. Cascaded PI controls scheme of PMDC motor

By substituting Equation (3) into Equation (2) and equating it to the voltage equation (1) allows the entire cascaded PI structure to be merged with the motor dynamics. The result is a single differential equation that represents the closed-loop system:

$$\begin{aligned} &K_{pi}(K_{p\omega}(\omega_{ref} - \omega) + K_{i\omega} \int (\omega_{ref} - \omega) dt - i_a) + \\ &K_{ii}(K_{p\omega} \int (\omega_{ref} - \omega) dt + K_{i\omega} \int (\omega_{ref} - \omega)\, dt - i_a)\, dt \\ &\quad = R_a i_a + L_a \frac{d}{dt} i_a + K_e \omega \end{aligned} \tag{4}$$

This expression combines the dynamic response of the electrical system, the current controller, and the speed controller into a unified formulation. The mechanical dynamics of the motor are also considered through the rotational equation:

$$J \frac{d}{dt}\omega + B\,\omega = K_t\, i_a \tag{5}$$

where J is the rotor inertia, B is the viscous damping coefficient, and K_t is the torque constant.

Therefore, the equations above represent the complete nonlinear model of the cascaded PI-controlled PMDC motor system. This formulation is particularly suitable for simulation and control design purposes, including linearization and state-space representation in subsequent analysis stages.

3.2. Proposed AVPSO strategy.

The AVPSO algorithm is designed to balance exploration and exploitation by dynamically updating its key parameters. The position and velocity of each particle in the swarm are iteratively updated according to the following equations:

$$v_i^{k+1} = w^k \cdot v_i^k + c_1^k \cdot r_1 \circ (p_i^k - x_i^k) + c_2^k \cdot r_2 \circ (g^k - x_i^k) \tag{6}$$

$$x_i^{k+1} = x_i^k + v_i^{k+1} \tag{7}$$

Here, x_i^k and v_i^{k+1} are the position and velocity vectors of the i^{th} particle at iteration k, respectively; $p_i^k$is the personal best position of the i^{th} particle up to k; $g^k$is the global best position found by the entire swarm up to k; r_1, r_2~U(0,1) are vectors of random scalars that are sampled uniformly; $\circ$ denotes element-wise multiplication; w^k is the inertia weight controlling the trade-off between global and local exploration; and c_1^k and c_2^k are the adaptive cognitive and social acceleration coefficients, respectively.

The w^k term is linearly decreased at each iteration according to:

$$w^k = w_{max} - \left(\frac{w_{max} - w_{min}}{k_{max}}\right) \cdot k \tag{8}$$

Where w_{max} =0.8, w_{min} =0.3, and k_{max} denoting the maximum number of iterations. The cognitive and social acceleration coefficients are also updated dynamically at each iteration using:

$$c_1^k = 2.5 - 2.0 \frac{k}{k_{max}} \tag{9}$$

$$c_2^k = 0.5 + 2.0 \cdot \frac{k}{k_{max}} \tag{10}$$

Therefore, this adaptive scheduling gradually shifts the swarm behavior from individual exploration (c_1^k) toward global convergence (c_2^k) as the iteration progresses [22,23].

The updated position of each particle is constrained by boundary conditions as follows:

$$x_i^{k+1} = min\left(max\left(x_i^{k+1}, lb\right), ub\right) \quad (11)$$

where lb and ub represent the lower and upper bounds of the search space, respectively. The optimization process terminates when either the maximum number of iterations $k_{\max}$ is reached or the change in the global best cost $|J^k - J^{k-1}|$ falls below a predefined threshold ε over several consecutive iterations, indicating convergence.

In AVPSO, the optimization is guided by a scalar objective function that quantifies the performance of each candidate solution. For PI controller tuning in the PMDC drive system, the objective function is defined to penalize both steady-state and transient errors in the electrical and mechanical responses. Specifically, the objective function is expressed as:

$$J(\theta) = E_\omega + E_{i_a} \quad (12)$$

where, $\Theta \in R^n$ represents the decision variables, typically control parameters such as gains or time constants, E_ω is the accumulated error in angular velocity, and $E_{i_a}$is the accumulated error in armature current, both error terms are computed over a fixed simulation or control horizon. However, the weighting factors in the cost function are set equally (both equal to one) in this study. This reflects driving scenarios where speed regulation and current control are given equal priority to achieve accurate tracking and maintain motor efficiency. Since the objective is to enhance overall dynamic and steady-state performance, both E_ω, and E_{ia} are treated with the same importance in the optimization process. Therefore, each component is defined as:

$$E_\omega = \int \left(\omega_{ref} - \omega\right)^2 dt \quad (13)$$

$$E_{i_a} = \int \left(i_{a-ref} - i_a\right)^2 dt \quad (14)$$

Therefore, the scalar cost function directs AVPSO toward parameter sets that achieve fast and accurate dynamic responses by minimizing overshoot and steady-state error [16].

Constraints on system parameters and dynamic behavior are handled within the AVPSO framework using a combination of bounded search space enforcement and simulation-based feedback. Each decision variable is confined to a predefined range:

$$\theta_j \in \left[\theta_j^{min}, \theta_j^{max}\right], j = 1, 2, \ldots, n \quad (15)$$

For ensuring the search remains within the feasible solution space, each position of the particle is adjusted after every update using boundary projection:

$$\theta_j^{k+1} = min\left(max\left(\theta_j^{k+1}, \theta_j^{min}\right), \theta_j^{max}\right) \quad (16)$$

Therefore, this constraint-handling strategy effectively prevents the optimizer from exploring invalid regions of the search space

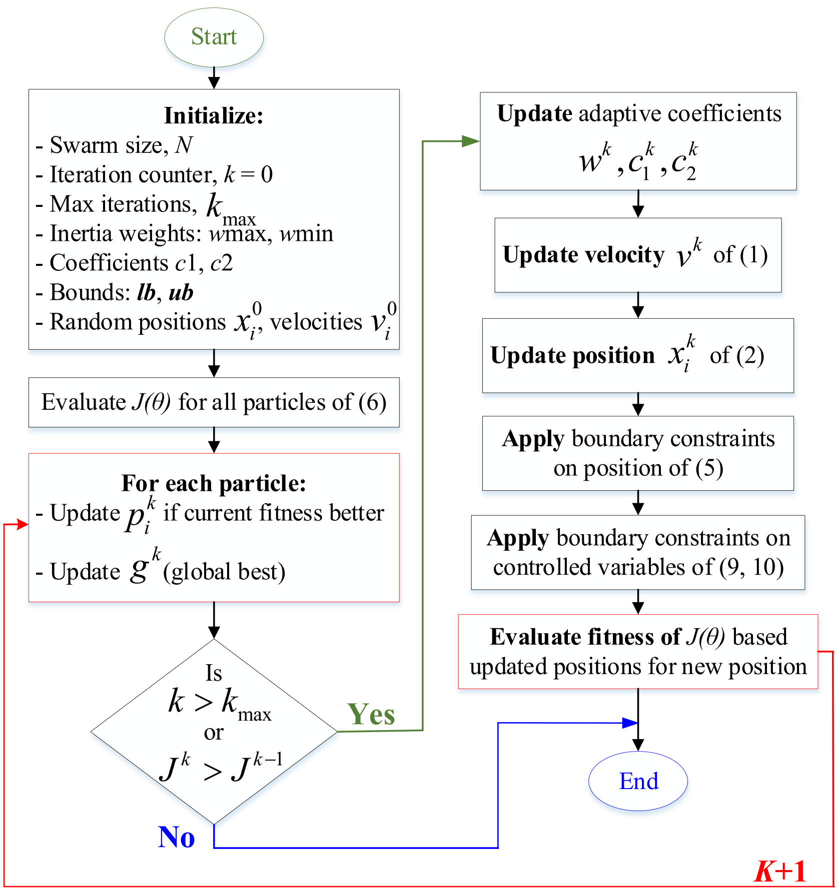

Figure 3. Flowchart of the adaptive variable PSO algorithm

Table 3. *Comparison of the proposed adaptive PSO and classical PSO Features*

Feature	Adaptive PSO	Classical PSO
Adaptive inertia w	Yes	No
Adaptive c1, c2	Yes	No
Cost history	Yes	No
Early stopping	Yes	No
More exploration	Yes	No
Practical convergence	High	Low

and contributes to the overall stability and convergence of the optimization process[24,25].

The dynamic system model evaluates the fitness function while implicitly satisfying physical and operational constraints such as current limits, voltage saturation, and speed thresholds. These constraints are not enforced explicitly but are reflected through simulation feedback. If a given parameter set leads to instability or violates system limits, the objective function $J(\theta)$ yields a high cost. This formulation enables AVPSO to reject infeasible solutions and favor parameter sets that result in stable and accurate system behavior[22,25].

Figure 3 shows the flowchart of the AVPSO algorithm. The process begins with initialization of particle positions and velocities within defined bounds. At each iteration, inertia weight and acceleration coefficients are updated adaptively. The fitness of each particle is evaluated using the objective function, and personal and global best positions are updated accordingly. This process continues until either the cost improvement becomes negligible over successive iterations or the maximum number of iterations is reached.

Table 3 summarizes the main differences between the proposed APSO and the classical PSO approach. The adaptive version integrates features such as dynamic adjustment of inertia weight, cognitive and social coefficients, and cost history tracking. These enhancements improve its capability to explore the solution space effectively and achieve faster, more reliable convergence.

In contrast, the classical PSO lacks these adaptive mechanisms and typically exhibits lower convergence speed and limited exploration space.

The proposed AVPSO and classical PSO methods were compared via a performance evaluation in which a PMDC drive system was modeled using the MATLAB/Simulink environment. The key parameters of the motor and the PSO techniques are listed in Table 4. The initial gains of the four PI controllers, namely, the proportional and integral gains for both the velocity and armature current loops, were randomly generated for both optimization methods. These gains were selected within the same predefined ranges. Specifically, the lower limits were set to 1, 0.1, 1, and 1, while the upper limits were set to 300, 5, 50, and 200, respectively. These limits ensured that both techniques were evaluated over an identical search space, providing a fair and consistent basis for performance comparison.

Meanwhile, the cost function defined in Equation (12) guides the optimization process. Therefore, the procedure is executed with a population size of 50 and a maximum of 100 generations, as illustrated in Figure 4.

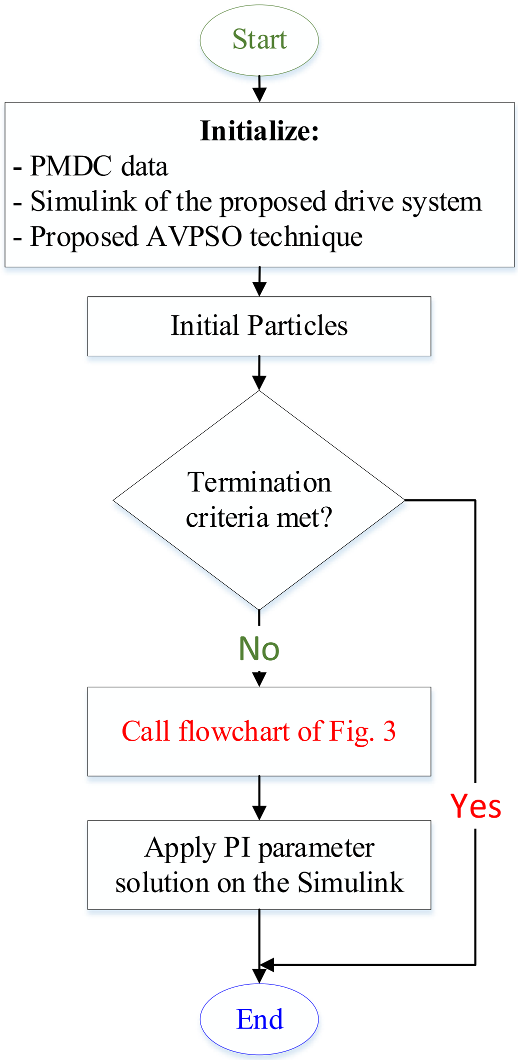

Figure 4. Implementation of the off-line AVPSO technique for optimizing the PI Parameters

4. RESULTS AND DISCUSSION

4.1. Comparison between AVPSO and PSO. A comparison between the proposed AVPSO technique and the classical PSO technique is presented in this section. Figure 5 presents the convergence behavior of the cost function for both the classical PSO and the proposed AVPSO. Although both methods achieved the same final cost value of 1,000,000, AVPSO converged faster, terminating at the 51st iteration.

Figure 6 illustrates the variations in the cognitive acceleration coefficient, social acceleration coefficient, and inertia weight throughout the AVPSO process. The adaptive behavior of these parameters enhances the balance between exploration and exploitation during tuning. Thus, the PI controller parameters obtained using each method differ, as listed in Table 5.

Although the cost function converges to the same value for both the AVPSO and classical PSO, this does not imply that the resulting PI controller parameters are identical. The cost

Table 4. *Key parameters of the motor drive system and PSO techniques*

Symbols	Name	Value	Unit
R_a	armature resistance	0.24	Ω
L_a	armature inductance	18	mH
K_e	back electromotive fore constant	0.7237	V · s/rad
K_t	torque constant	0.7237	N · m/A
B	viscous damping coefficient	0.01	N · m · s/rad
J	moment of inertia	0.5	$Kg.m^2$
N	number of particles (swarm size)	50	particles
C_1	cognitive acceleration coefficient of classical PSO	0.5	-
C_2	social acceleration coefficient of classical PSO	0.5	-
w	inertia weight of classical PSO	0.2	-
w_{max}	maximum inertia weight of proposed AVPSO	0.8	-
w_{min}	minimum inertia weight of proposed AVPSO	0.3	-

function evaluates the overall system performance based on predefined criteria such as tracking error, control effort, and response time. Because the optimization landscape may contain multiple parameter sets that yield similar cost values, each algorithm can converge to a different solution that satisfies the objective equally well. In the case of AVPSO, the dynamic adjustment of the inertia weight and acceleration coefficients enhances search-space exploration. This adaptive behavior enables AVPSO to identify distinct, yet equally optimal, PI parameter sets compared to classical PSO. The following section presents two numerical scenarios for a further comparison of the PMDC motor performance under both tuning methods.

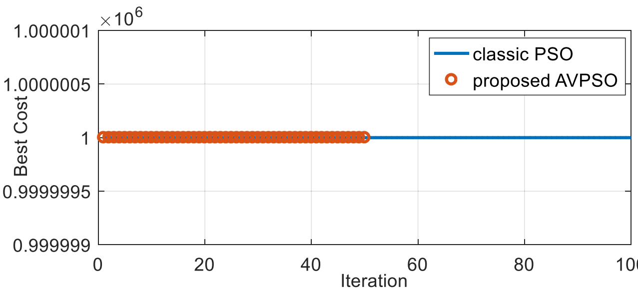

Figure 5. Cost function convergence of classical PSO and proposed AVPSO

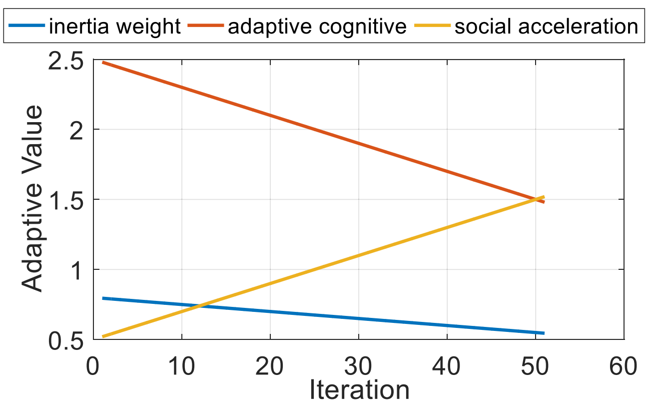

Figure 6. Implementation of the off-line AVPSO technique for optimizing the PI Parameters

4.2. Four quadrant operation scenario. Figures 7–9 compare the PMDC motor performance under a four-quadrant operation scenario using the proposed AVPSO-based PI tuning method and the classical PSO approach. In this setup, the reference traction torque is maintained at 7 Nm, while the angular velocity alternates between 600 RPM (62.83 rad/s) in both forward and reverse directions. The analysis focuses on system behavior during quadrant transitions and dynamic responses.

As shown in Figure 7, the armature voltage maintains the correct polarity and magnitude across all quadrants. In forward operation, the voltage reaches a peak of 48.5 V for both tuning methods. In the reverse operation, the AVPSO method yields a peak of –48.8 V, compared to –42.5 V for classical PSO. These results indicate that AVPSO provides more symmetrical and consistent voltage regulation throughout the operating range. The AVPSO method showed a sharper voltage spike at 12 s during the quadrant transition (Figure 7(a)). This is attributed to the rapid response to error changes. Despite the higher transient, the system remains stable, as evidenced by the smooth settling in the angular velocity (Figure 7(b)), armature current (Figure 7(c)), and torque (Figure 7(d)), with no signs of instability or oscillatory behavior.

The angular-velocity response (Figure 7(b)) confirms that the improved dynamic performance of the proposed AVPSO-based tuning method is comparable to that of PSO. In the forward rotation, the settling time was reduced by 15.6%, reaching approximately 6.2 s. In the reverse rotation, the settling time decreased

Table 5. *Optimized PI controller parameters*

	Proposed AVPSO	Classic PSO
$K_{p\omega}$	227.8	123.2
$K_{i\omega}$	1.1	1.1
K_{pi}	23.8	6.9
K_{ii}	182.4	5.1

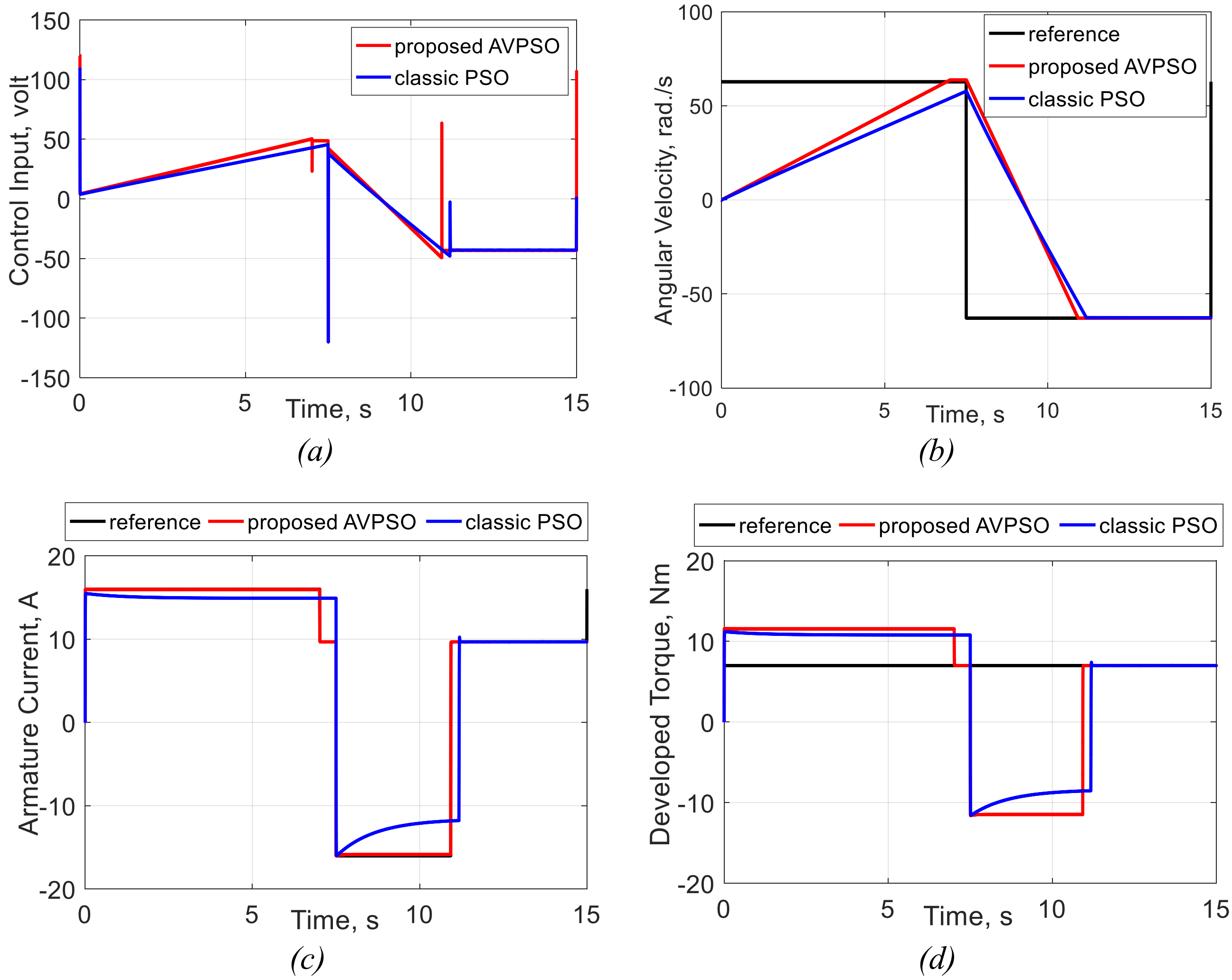

Figure 7. (a) Armature voltage, (b) angular velocity, (c) armature current, and (d) developed torque under four-quadrant operation

by 2.1%, achieving a value of approximately 3.26 s. Additionally, the AVPSO method eliminates steady-state error in both directions, whereas the classical PSO method shows a 6.2 rad/s error during forward operation.

The armature current response (Figure 7(c)) further highlights the advantages of the proposed method. The outer PI controller generated reference currents of 16 and 9.7 A for the forward and reverse motions, respectively. Under classical PSO tuning, the actual current failed to accurately track the reference during transients and exhibited a steady-state error of 1.02 A in forward operation. In contrast, AVPSO ensures precise current tracking with no steady-state errors, even during dynamic transitions. These improvements in current and voltage behaviors enhance both the electrical input power and mechanical output power. In motoring mode, AVPSO ensures smooth energy delivery, whereas in regenerative mode, it handles the reverse energy flow more effectively, as evidenced by the higher and more stable negative voltage.

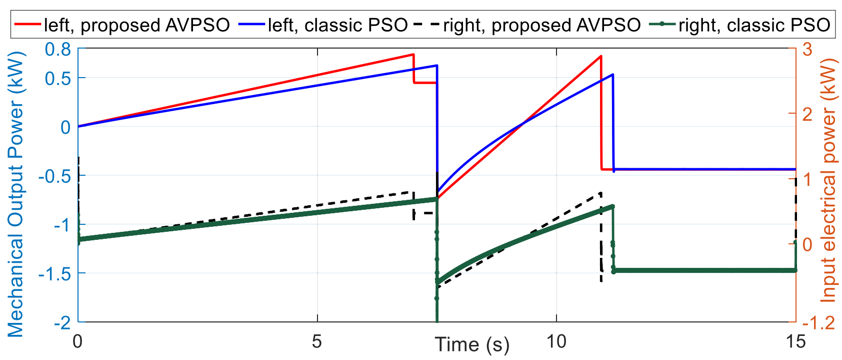

Figure 8. Power consumption under four-quadrant operation

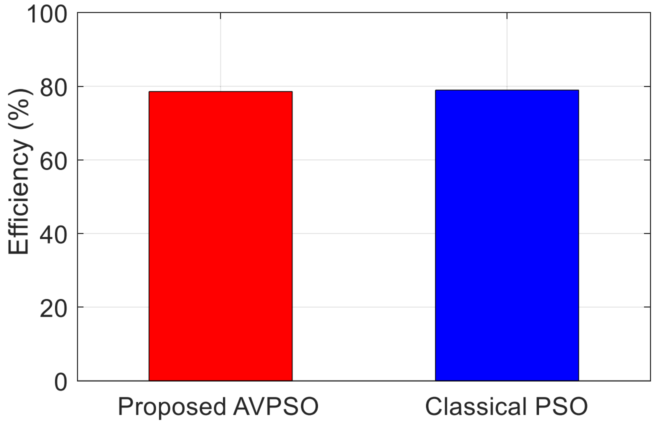

Figure 9. Motor efficiency under four-quadrant operation

As shown in Figure 7(d), the developed torque reaches the reference value more quickly for AVPSO than PSO, with faster responses by 0.5 and 1 s in the forward and reverse directions, respectively. Figure 8 further demonstrates that AVPSO improves energy efficiency with reduced power consumption during both motoring and regenerative operations. Moreover, Figure 9 shows that the AVPSO method achieves better dynamic performance with faster settling, improved tracking, and elimination of steady-state errors, while maintaining a motor efficiency comparable to classical PSO at 78.8%, indicating no significant gain in steady-state efficiency. Finally, Table 6 summarizes the performance indicators for both tuning techniques under a four-quadrant operation scenario.

4.3. Torque disturbance operation scenario.

Figures 10–12 illustrate the PMDC motor response under a torque-disturbance scenario by comparing the performance of the proposed AVPSO-based PI tuning with that of classical PSO. Following the standard-load case, this scenario was used to evaluate motor performance under more demanding torque conditions to assess the dynamic response and energy-conversion efficiency of both tuning methods. As shown in Figure 10(a), the armature voltage during forward operation remains positive, peaking at approximately 95 V for AVPSO and 97 V for classical PSO. Although the PSO method yields a slightly higher peak voltage, AVPSO results in a faster and more stable response to sudden changes in torque demand. In addition, a more pronounced voltage spike at 12 s was observed using AVPSO because of its faster corrective action during the sudden torque reduction. This aggressive response improves error minimization but leads to a transient overshoot. However, as seen in the corresponding angular velocity (Figure 10(b)), armature current (Figure 10(c)), and torque (Figure 10(d)) plots, the voltage stabilizes quickly without introducing oscillations, confirming that the system stability was maintained.

Figure 10(b) shows the angular velocity response, where the proposed AVPSO method demonstrates enhanced performance under high-torque conditions. Compared to PSO, the settling time using AVPSO was reduced by 10.7%, reaching approximately 10.3 s. In addition, the steady-state error was significantly reduced . The classical PSO resulted in a steady-state error of 7.7 rad/s, whereas AVPSO reduced this value to 3.7 rad/s, indicating superior speed regulation.

Figures 10–12 illustrate the PMDC motor response under a torque-disturbance scenario by comparing the performance of the proposed AVPSO-based PI tuning with that of classical PSO. Following the standard-load case, this scenario was used to evaluate motor performance under more demanding torque conditions to assess the dynamic response and

Table 6. *Performance comparison under four-quadrant operation*

Performance Metric	AVPSO-Based Tuning	Classical PSO-Based Tuning	Observation
Peak Armature Voltage (Forward)	48.5 V	48.5 V	Same performance
Peak Armature Voltage (Reverse)	–48.8 V	–42.5 V	AVPSO shows better symmetry in voltage regulation
Settling Time (Forward)	6.2 s	~7.35 s	AVPSO reduced time by 15.6%
Settling Time (Reverse)	3.26 s	~3.33 s	AVPSO reduced time by 2.1%
Speed Steady-State Error (Forward)	0 rad/s	6.2 rad/s	AVPSO eliminates steady-state error
Armature Current Tracking Error	0 A	1.02 A (forward)	AVPSO achieves accurate current tracking
Torque Response Time (Forward)	Faster by 0.5 s	Slower	AVPSO responds quicker
Torque Response Time (Reverse)	Faster by 1.0 s	Slower	AVPSO responds quicker
Power Consumption	Higher during transitions	Lower	AVPSO enhanced motor performance without compromising the efficiency of classic PSO technique
Motor Efficiency	78.8%	78.8%	Comparable for both techniques

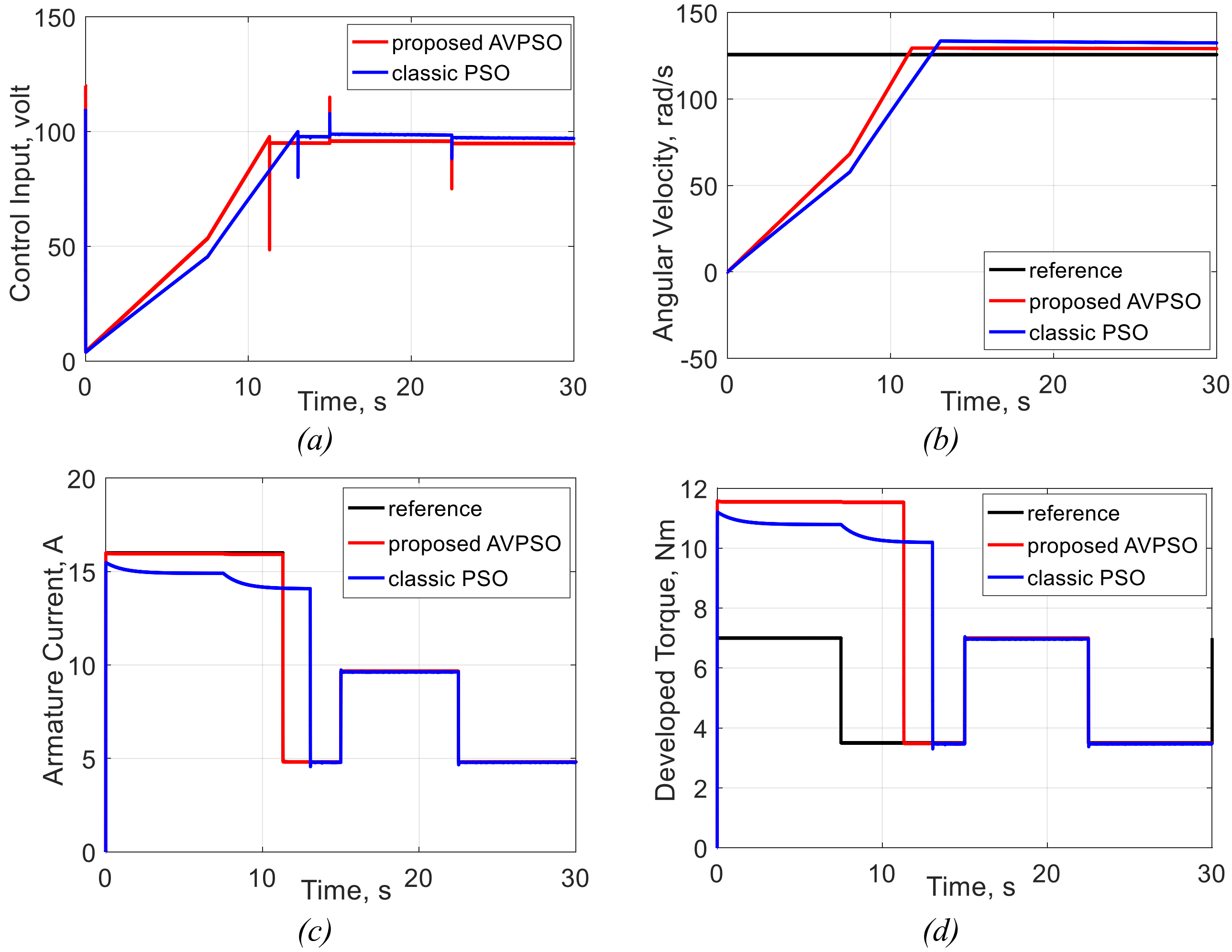

Figure 10. (a) Armature voltage, (b) angular velocity, (c) armature current, and (d) developed torque under torque-disturbance operation

energy-conversion efficiency of both tuning methods. As shown in Figure 10(a), the armature voltage during forward operation remains positive, peaking at approximately 95 V for AVPSO and 97 V for classical PSO. Although the PSO method yields a slightly higher peak voltage, AVPSO results in a faster and more stable response to sudden changes in torque demand. In addition, a more pronounced voltage spike at 12 s was observed using AVPSO because of its faster corrective action during the sudden torque reduction. This aggressive response improves error minimization but leads to a transient overshoot. However, as seen in the corresponding angular velocity (Figure 10(b)), armature current (Figure 10(c)), and torque (Figure 10(d)) plots, the voltage stabilizes quickly without introducing oscillations, confirming that the system stability was maintained.

Figure 10(b) shows the angular velocity response, where the proposed AVPSO method demonstrates enhanced performance under high-torque conditions. Compared to PSO, the settling time using AVPSO was reduced by 10.7%, reaching

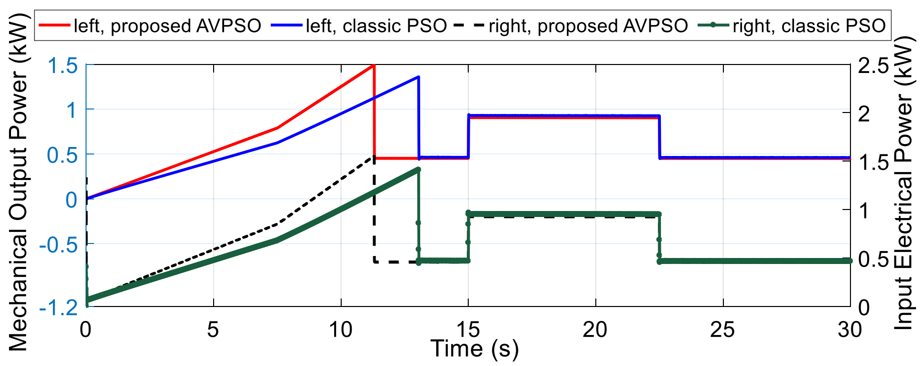

Figure 11. Power consumption under torque disturbance operation

approximately 10.3 s. In addition, the steady-state error was significantly reduced. The classical PSO resulted in a steady-state error of 7.7 rad/s, whereas AVPSO reduced this value to 3.7 rad/s, indicating superior speed regulation.

The good performance of AVPSO is further supported by the armature current response, as shown in Figure 10(c). The outer PI controller assigned reference current values of 16 and 4.7 A in the forward and reverse directions, respectively. Under classical PSO tuning, the motor current deviates from the reference value during transients and exhibits a steady-state error of approximately 1 A. In contrast, AVPSO achieved accurate current tracking with no steady-state error, even under dynamic conditions.

Based on the behavior of both the voltage and current, the electrical input power and mechanical output power can be inferred. During motoring mode, AVPSO ensures a smooth and consistent power profile, contributing to efficient energy transfer. Although the regenerative operation is less dominant in this scenario, the controller maintains a stable reverse energy flow and operational reliability when required.

As shown in Figure 10(d), the developed torque reaches the reference value 1.7 s faster with AVPSO than with the classical PSO, and exhibits reduced oscillations during convergence. Consequently, the power consumption response in Figure 11 is more efficient and stable under AVPSO control, indicating improvements in both transient and steady-state operations. Moreover, Figure 12 shows that the AVPSO method achieves superior dynamic performance with faster settling, improved tracking, and reduced steady-state error, while maintaining a motor efficiency comparable to that of classical PSO at approximately 91.0%, i.e., no significant gain in steady-state efficiency. Finally, Table 7 summarizes the key performance indicators for both tuning techniques under the torque–disturbance scenario.

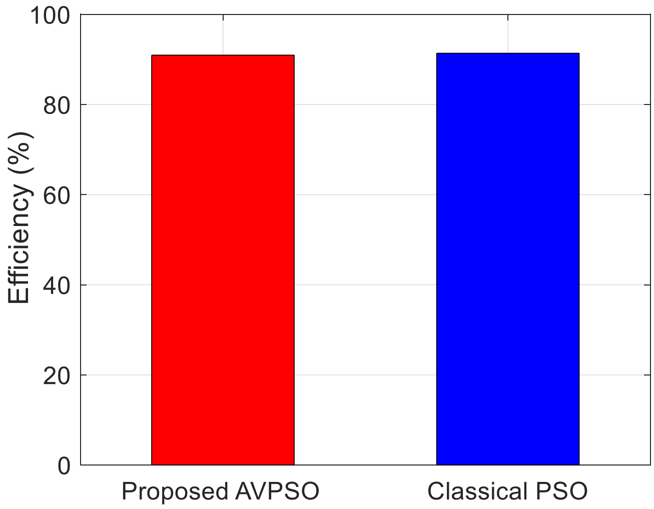

Figure 12. Motor efficiency under torque disturbance operation

4.4. Comparison with existing PSO-based PI tuning methods. Table 8 compares PSO-based PI/PID tuning methods for PMDC drives. Previous studies have shown that traditional PSO improves dynamic tracking, reduces overshoot, and handles load transients more effectively than manual tuning or GA-based optimization[26–28]. However, these approaches rely on static PSO parameters and do not consider four-quadrant operations, transient load variations, or the trade-off between speed and current errors through weighted tuning. In contrast, our AVPSO method introduces adaptive velocity update parameters, achieving faster convergence and improved tracking while maintaining comparable motor efficiency (~78–91%) while ensuring stability under regenerative-braking and torque-disturbance conditions.

Table 7. *Performance Comparison under Torque Disturbance Scenario*

Performance Metric	AVPSO-Based Tuning	Classical PSO-Based Tuning	Observation
Peak Armature Voltage (Forward)	~95 V	~97 V	Classical yields slightly higher peak, but less stable
Settling Time (Angular Velocity)	10.3 s	~11.54 s	AVPSO reduces time by 10.7%
Speed Steady-State Error	3.7 rad/s	7.7 rad/s	AVPSO shows better speed regulation
Armature Current Tracking Error	0 A	~1 A	AVPSO achieves accurate current tracking
Torque Response Time	Faster by 1.7 s	Slower	AVPSO reaches reference torque sooner
Torque Oscillation	Reduced	Noticeable	AVPSO shows smoother convergence
Power Consumption	Higher during transitions	Lower	AVPSO technique enhanced motor performance without compromising the efficiency of classic PSO technique
Motor Efficiency	91.0%	91.0%	Comparable efficiency for both techniques

Table 8. *Summary of selected PSO-based PI/PID tuning methods for PMDC motor drives*

Reference	Control Structure	Objective (Cost)	Gains over classical tuning	How it differs from your AVPSO
[26]	Triloop PID (hysteretic control of firing angle)	Minimize $e_\omega + e_I + e_R$ (singleweight sum of speed, current deviation, ripple)	Smoother start torque, fast acceleration, stable trajectory tracking vs classical tuning	No adaptation of PSO coefficients (fixed w,c_1,c_2); optimization of three loops only; no fourquadrant effort; no explicit efficiency reporting
[27]	Triloop errordriven PID	Integral of timesquared error; dynamic error criterion	Improved transient, fast settling (~4 s), zero overshoot under load/disturbance	Standard PSO; no adaptive velocity; performance verified in simulation only; various transient scenarios, but no regenerative mode
[28]	Cascade P + PI (no ripple loop, only current and speed)	Integral time absolute error over speed and position errors under load conditions	PSO eliminated position overshoot (vs ~7 % class., ~4 % genetic algorithm) and suppressed deviation ~12.0°under loaded start	Only two PI loops; constant PSO; no fourquadrant or regenerative analysis; emphasis on overshoot; no torque disturbance scenario

5. CONCLUSIONS

This study developed an AVPSO approach for tuning PI controllers of a PMDC motor-drive system for LEVs. This method introduces an adaptive adjustment of the inertia weight and acceleration coefficients to improve convergence and parameter tuning. The simulation results demonstrate that AVPSO-based tuning enhances the key system performance parameter. The classical PSO method exhibited residual speed and current errors during forward operation, whereas the AVPSO achieved a 15.6% reduction in settling time and eliminated steady-state errors in both rotational directions. In addition, the AVPSO approach improves the quality of the power consumption response during transient events, particularly under regenerative braking. However, it is important to note that both methods maintained comparable motor efficiencies, with no significant efficiency gains with the proposed method. These findings confirm that the AVPSO algorithm provides an accurate and responsive control strategy for PI parameter optimization in LEV drive systems. Its effectiveness in reducing tracking errors and enhancing the dynamic behavior supports its applicability for intelligent controller designs.

In future work, the proposed cost function will be further developed to enable online computation of the drive controller parameters. This enhancement will enable the control system to adapt in real-time under varying loads and operating conditions in practical LEV applications. Additionally, experimental validation through HIL testing will be performed to assess the system stability and implementation feasibility.

AFFILIATIONS AND AUTHOR DETAILS

Undergraduate Author

Mohammed Aldhaif Allah – *Control and Instrumentation Engineering Department, King Fahd University of Petroleum & Minerals, Dhahran 31261, Saudi Arabia;* 0009-0003-7275-5824
Email: s202274560@kfupm.edu.sa

Corresponding Author

Moustafa Magdi Ismail – *Research Mentor, Interdisciplinary Research Center for Sustainable Energy Systems (IRC-SES), King Fahd University of Petroleum & Minerals, Dhahran 31261, Saudi Arabia;* 0000-0001-5554-6084
Email: moustafa.mohamed@kfupm.edu.sa

ACKNOWLEDGEMENTS

This research is a direct outcome of an internal project (INSE2521), conducted at the Interdisciplinary Research Center for Sustainable Energy Systems (IRC-SES), King Fahd University of Petroleum & Minerals, Dhahran 31261, Saudi Arabia. The authors sincerely appreciate the support and resources provided by the IRC-SES, which contributed significantly to the successful completion of this work.

REFERENCES

(1) D. Rimpas, S. D. Kaminaris, D. D. Piromalis, G. Vokas, K. G. Arvanitis, and C.-S. Karavas, “Comparative Review of Motor Technologies for Electric Vehicles Powered by a Hybrid Energy Storage System Based on Multi-Criteria Analysis,” Energies, vol. 16, p. 2555, 2023.

(2) A. Eldho Aliasand and F. T. Josh, “Selection of Motor foran Electric Vehicle: A Review,” Materials Today: Proceedings, vol. 24, pp. 1804–1815, 2020/01/01/ 2020.

(3) A. Joseph Godfrey and V. Sankaranarayanan, “A new electric braking system with energy regeneration for a BLDC motor driven electric vehicle,” Engineering Science and Technology, an International Journal, vol. 21, pp. 704–713, 2018/08/01/ 2018.

(4) A. Isah, A. Mohammed, and A. Hamza, “Electric Power-Assisted Steering: A Review,” in 2019 2nd International Conference of the IEEE Nigeria Computer Chapter (NigeriaComputConf), 2019, pp. 1–6.

(5) E. Sangeetha and V. Ramachandran, “Different topologies of electrical machines, storage systems, and power electronic converters and

their control for battery electric vehicles—a technical review," Energies, vol. 15, p. 8959, 2022.

(6) T. Sutikno, N. R. N. Idris, and A. Jidin, "A review of direct torque control of induction motors for sustainable reliability and energy efficient drives," Renewable and Sustainable Energy Reviews, vol. 32, pp. 548–558, 2014/04/01/ 2014.

(7) W. Słowik, P. Piątek, T. Dziwiński, and J. Baranowski, "Selected current sensing circuits for motor control application," Pomiary Automatyka Robotyka, vol. 21, 2017.

(8) Z. Bitar, A. Sandouk, and S. Al Jabi, "Testing the performances of DC series motor used in electric car," Energy Procedia, vol. 74, pp. 148–159, 2015.

(9) N. M. Morris and N. M. Morris, "DC Machines," Electrical Principles III, pp. 44–63, 1978.

(10) E. Soressi, "New life for old compound DC motors in industrial applications?," in 2012 IEEE International Conference on Power Electronics, Drives and Energy Systems (PEDES), 2012, pp. 1–6.

(11) Y. S. Chang, Y. C. Luo, and P. C. Shih, "AIR: Agent and Ontology-Based Information Retrieval Architecture for Mobile Grid," in 2008 IEEE Asia-Pacific Services Computing Conference, 2008, pp. 650–655.

(12) M. Onda, M. Misawa, T. Kojima, N. Aya, A. Seto, and T. Yamane, "A stratospheric LTA stationary platform for telecommunication and environmental protection," in SICE '99. Proceedings of the 38th SICE Annual Conference. International Session Papers (IEEE Cat. No.99TH8456), 1999, pp. 1227–1232.

(13) W. Xu, M. M. Ismail, Y. Liu, and M. R. Islam, "Parameter optimization of adaptive flux-weakening strategy for permanent-magnet synchronous motor drives based on particle swarm algorithm," IEEE Transactions on Power Electronics, vol. 34, pp. 12128–12140, 2019.

(14) M. M. Ismail, M. Al-Dhaifallah, H. Rezk, H. U. Rahman Habib, and S. A. Hamad, "Optimizing battery discharge management of PMSM vehicles using adaptive nonlinear predictive control and a Generalized Integrator," Ain Shams Engineering Journal, p. 103169, 2024/11/19/ 2024.

(15) Y. Yu, Y. Pan, Q. Chen, Y. Hu, J. Gao, Z. Zhao, et al., "Multi-Objective Optimization Strategy for Permanent Magnet Synchronous Motor Based on Combined Surrogate Model and Optimization Algorithm," Energies, vol. 16, p. 1630, 2023.

(16) L. Kong, H. Zhang, T. Zhang, J. Wang, C. Yang, and Z. Zhang, "Adaptive Control Parameter Optimization of Permanent Magnet Synchronous Motors Based on Super-Helical Sliding Mode Control," Applied Sciences, vol. 14, p. 10967, 2024.

(17) H. Xu, J. Zhang, J. Liu, Y. Cao, and A. Ma, "Optimization of Ship Permanent Magnet Synchronous Motor ADRC Based on Improved QPSO," Applied Sciences, vol. 15, p. 1608, 2025.

(18) G. Yuan, Y. Tao, S. Bozhko, P. Wheeler, T. Dragicevic, and C. Gerada, "Neural Network aided PMSM multi-objective design and optimization for more-electric aircraft applications," Chinese Journal of Aeronautics, vol. 35, pp. 233–246, 2022.

(19) C. Sun, F. Wen, W. Xiong, H. Wang, and H. Shang, "Multi-objective comprehensive teaching algorithm for multi-objective optimisation design of permanent magnet synchronous motor," IET Electric Power Applications, vol. 14, pp. 2564–2576, 2020.

(20) M. M. Ismail, W. Xu, X. Wang, A. K. Junejo, Y. Liu, and M. Dong, "Analysis and optimization of torque ripple reduction strategy of surface-mounted permanent-magnet motors in flux-weakening region based on genetic algorithm," IEEE Transactions on Industry Applications, vol. 57, pp. 4091–4106, 2021.

(21) N. Pragallapati, T. Sen, and V. Agarwal, "Adaptive Velocity PSO for Global Maximum Power Control of a PV Array Under Nonuniform Irradiation Conditions," IEEE Journal of Photovoltaics, vol. 7, pp. 624–639, 2017.

(22) M. P. Aghababa, A. M. Shotorbani, and R. M. Shotorbani, "An Adaptive Particle Swarm Optimization Applied to Optimum Controller Design for AVR Power Systems," International Journal of Computer Applications, vol. 11, pp. 22–29, 2010.

(23) X. Li, K. Mao, F. Lin, and X. Zhang, "Particle swarm optimization with state-based adaptive velocity limit strategy," Neurocomputing, vol. 447, pp. 64–79, 2021.

(24) A. R. Jordehi, "A review on constraint handling strategies in particle swarm optimisation," Neural Computing and Applications, vol. 26, pp. 1265–1275, 2015.

(25) M. S. Innocente and J. Sienz, "Constraint-handling techniques for particle swarm optimization algorithms," arXiv preprint arXiv:2101.10933, 2021.

(26) A. M. Sharaf and A. A. A. El-Gammal, "A novel Particle Swarm Optimization PSO tuning scheme for PMDC motor drives controllers," in Proc. Int. Conf. Power Eng., Energy and Electr. Drives, 2009, pp. 134–139.

(27) P. G. Medewar and R. K. Munje, "PSO-based PID controller tuning for PMDC motor," in Proc. Int. Conf. Energy Systems and Applications (ICESA), 2015, pp. 522–526.

(28) K. G. Abdulhussein, N. M. Yasin, and I. J. Hasan, "Comparison of cascade P-PI controller tuning methods for PMDC motor based on intelligence techniques," Int. J. Electr. Comput. Eng. (IJECE), vol. 12, p. 1, 2022.